Microstructural and load hold effects on small fatigue crack growth in $\alpha+\beta$ dual phase Ti alloys

S. Hémery, J.C. Stinville

Version of Record: https://www.sciencedirect.com/science/article/pii/S0142112321005405
Manuscript_6595e5b06400c6cd2956cf431c660dbf

Microstructural and load hold effects on small fatigue crack growth in α+β dual phase Ti alloys

S. Hémery[a,*], J.-C. Stinville[b]

[a] Institut Pprime, ISAE-ENSMA, Université de Poitiers, CNRS UPR 3346, Téléport 2, 1 avenue Clément Ader, BP 40109, Futuroscope-Chasseneuil Cedex, 86961, France

[b] Departments of Materials Science and Engineering, University of Illinois at Urbana-Champaign, Urbana, IL, USA

[*] samuel.hemery@ensma.fr

Abstract

Microstructurally small crack growth was monitored in Ti-6Al-4V and Ti-6Al-2Sn-4Zr-2Mo with equiaxed and bi-modal microstructures. The influence of the microstructure was assessed to obtain an improved understanding of the lifetime variability observed in Ti alloys. Primary α grains, basal plane cracking and misalignment across boundaries were identified as key features for high crack growth rates. The origin of life debits encountered under dwell-fatigue loadings was also investigated through crack growth monitoring with the introduction of load holds at peaks stress. Dwell periods were found to induce a substantial small crack acceleration.

Keywords

Titanium alloys, low cycle fatigue, microstructure, fatigue crack growth, dwell-fatigue

Highlights

- The small fatigue crack growth (CG) was monitored in Ti alloys
- CG was faster in equiaxed α than in transformed β
- Well aligned basal planes with high Schmid factors lead to highest CG rates
- Load holds induced an substantial crack acceleration

1. Introduction

Titanium alloys are widely employed in aerospace applications owing to superior properties such as their specific strength and corrosion resistance [1]. Structural or gas turbine engines components generally experience cyclic loadings during aircraft operation [2]. The fatigue performance of Ti alloys is thus a critical property that has attracted numerous research efforts to overcome the challenges associated with its prediction. Significant complexity arise from the variety of dual phase microstructures obtained through different thermo-mechanical processing routes that influence the different stages of crack initiation and growth [3–6]. However, the specificities of local microstructural configurations result in a substantial fatigue-life variability that has to be accounted for in the component design [7–9]. In this context, fatigue crack nucleation mechanisms have received a continuous interest over the past decades [10–13]. In particular, recent studies have evidenced crack nucleation at (0001) twist boundaries in a variety of Ti alloys with different microstructures and testing conditions [11,14]. However, no analysis of cracks growing from such microstructural elements has been reported in the literature yet. Although it can consume a substantial part of the lifetime, early stages of crack extension across the microstructure and associated barriers are still not well documented. Such investigations are important to identify configurations leading to rapid or slow propagation of cracks, and offer insights into microstructure tailoring for fatigue resistant titanium alloys.

In particular, prior works have suggested that the small crack growth stage has a major contribution to the reduction in lifetime arising from the introduction of a load hold at peak stress in the cyclic loading of near-α Ti alloys [2,15,16].

Small cracks are characterized by a greater (or at least similar) crack growth rate than the corresponding long fatigue cracks subjected to the same nominal driving force [8,17]. Crack retardation and acceleration phenomena were also reported to occur in the small crack regime [18,19]. The scatter in growth rates can reach a decade in the low ΔK regime [20]. The microstructure plays a key role in the crack growth behavior through different lengthscales and phase arrangements found in engineering dual phase microstructures [21–23]. The pronounced deformation anisotropy of the dominant α phase is also of prime importance. In particular, crystallographic orientation [24–26] and active slip systems [24] have a major influence on the crack growth rates. These features also govern the transition between the two main crack growth modes: striated or facetted [15,16,27,28]. Finally, the substantial time dependent plastic strain accumulation reported to occur in Ti further complicates the picture [27]. The present work aims at advancing the understanding of small crack growth in Ti alloys, to clarify the associated consequences on the fatigue behavior.

The recent development of focused ion beam facilitates the studies of the small crack growth behaviors through controlled milling of initial defects [22,24,29–31]. With this technique, the effect of a specific microstructural barrier can be investigated [32]. A key role of microstructure (primary α or transformed β regions) as well as crystallographic orientations was evidenced using this method. However, the features of natural crack initiation sites, in terms of pre-existing dislocation structures, crystallography, geometry and phase arrangements, may not be properly accounted for with this approach. Alternatively, striations are often used for determining cracks growth rates and studying the role of the microstructure [15,33]. Nevertheless, prior studies have highlighted some limitations in the investigated regime as striations are not clearly generated for ΔK values lower than 10 $MPa\sqrt{m}$ [20], crack arrests can be difficult to identify and thousands of cycles can contribute to the formation of a single facet [34]. For these reasons, we have privileged a method based on growth monitoring of naturally initiated cracks using scanning electron microscopy (SEM) during interrupted cyclic loadings. This procedure also has several intrinsic limitations that will be discussed in the following sections.

In the present study, Ti-6Al-4V and Ti-6Al-2Sn-4Zr-2Mo dual phase titanium alloys with equiaxed and bi-modal microstructures were tested in the low cycle fatigue regime. The different compositions and microstructures were used to emphasize differences and similarities in small crack growth behavior. After cycling until crack nucleation, fatigue tests were repeatedly interrupted to monitor the early stages of growth of natural cracks using scanning electron microscopy (SEM). In addition to microstructure, crystallographic orientations were considered in the analysis using electron back-scattered diffraction (EBSD). The variety of microstructures, compositions and loading conditions investigated enabled to identify important features and to assess their influence on the growth behavior. As the fatigue performance of the Ti-6Al-2Sn-4Zr-2Mo alloy is known to be dwell sensitive [35,36], the effect of dwell-fatigue loadings on small crack growth was investigated in this alloy. The contribution of the small crack growth stage to the dwell-fatigue life debit is finally discussed in light of these results.

2. Material and experiments

Ti-6Al-2Sn-4Zr-2Mo (Ti-6242) and Ti-6Al-4V (Ti-64) alloys were employed in the present study. The compositions of these alloys are given in table 1. Micrographs showing the microstructures are presented in figure 1. The Ti-6242 alloy has a triplex microstructure composed of primary α grains and transformed β regions. In these regions, coarse lamellas are embedded within the residual β matrix where nano-scale α laths are present. Two variants of the Ti-64 alloy are used with equiaxed (Ti-64MTR) or bi-modal (Ti-64BM) microstructures. Average α grains size, associated surface fraction and average lamella thicknesses are presented in table 2. The reader is referred to [14] for additional details about the

microstructures. The Young's modulus, the yield strength, the ultimate tensile strength and the elongation are shown in table 3 for all materials. Tensile tests were carried out at room temperature using a strain rate of 10^{-2} s^{-1}. Such strain rate is similar to the loading rate used for cyclic tests. It is worth noting that the applied strain rate leads to strength values slightly higher than typical tensile properties obtained using quasi-static tests.

Alloy	Al	V	Sn	Zr	Mo	Si	Fe	O
Ti-6242	6.08	-	2.00	4.03	1.99	0.074	0.02	0.11
Ti-64BM	6.52	4.22	-	-	-	-	0.14	0.21
Ti-64MTR	6.28	4.09	-	-	-	-	< 0.19	0.18

Table 1: Composition of the alloys used in this work in weight % (Ti is balance)

Alloy	Primary α grain size (μm)	Primary α surface fraction (%)	Colony size (μm)	Lamella thickness (μm)	Nano-lamella thickness (μm)
Ti-6242	9.5	65	2.3	0.8	0.04
Ti-64BM	12.3	40	2.8	0.5	-
Ti-64MTR	3.4	-	-	-	-

Table 2: Microstructural features of the materials used in this work

Alloy	Young's modulus (GPa)	Yield strength (MPa)	Ultimate tensile strength (MPa)	Elongation (%)
Ti-6242	118	966	1013	13.7
Ti-64BM	118	998	1042	15.2
Ti-64MTR	104	993	1023	13.4

Table 3: Tensile properties with a strain rate of 10^{-2} s^{-1}

Fatigue tests were carried out using dogbone shaped specimens manufactured via electrical discharge machining. The gage length is 10 mm, the gage width of 2 mm and the initial thickness is about 1 mm. This geometry was selected to facilitate crack detection and growth monitoring using SEM, while considering a representative microstructural area. Both faces were first ground with SiC paper up to 4000 grade. A 9 μm diamond suspension was then used for rough polishing before a final step involving a mixture of 90 % suspension containing 0.04 μm silica particles and 10% H_2O_2. Homogeneous crack nucleation over the gage lengths demonstrates no major influence of edges on crack nucleation.

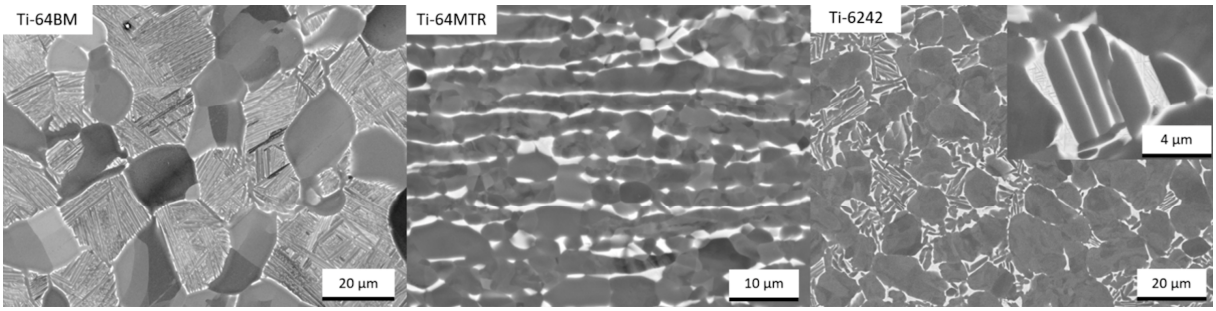

Figure 1: SEM micrographs showing the microstructure of the materials considered in the present study

Cyclic loadings were applied at room temperature using an Instron 8862 universal testing machine. The peak stress (σ_{max}) was held for 1 s during fatigue tests. 120 s load holds at peak stress were introduced in the loading waveform of a Ti-6242 specimen, to study the influence of load holds on crack growth. Loading and unloading were achieved in 1 s. The minimum stress, which is set at 10 % of σ_{max}, was held for 1 s. The fatigue loading waveform is shown schematically in figure 2a. An extensometer is used to continuously monitor strain accumulation. Most tests were carried out with the peak stress set at 90 – 87.5 % of the yield strength, which is given in table 3. However, additional tests were carried out with a higher peak stress (i.e. 95 % of the yield strength) to investigate the effect of load holds on crack growth in a regime favoring substantial dwell-debits [2,35]. The tests were interrupted before failure of the specimen. The

cumulated plastic strain is plotted as a function of the number of cycles in figure 2b. Testing was resumed to monitor the growth of nucleated cracks. No extensometer was used at this stage to preserve the cleanliness of the specimen surface. Therefore, the stress-strain curve beyond the first stop is not shown in figure 2b.

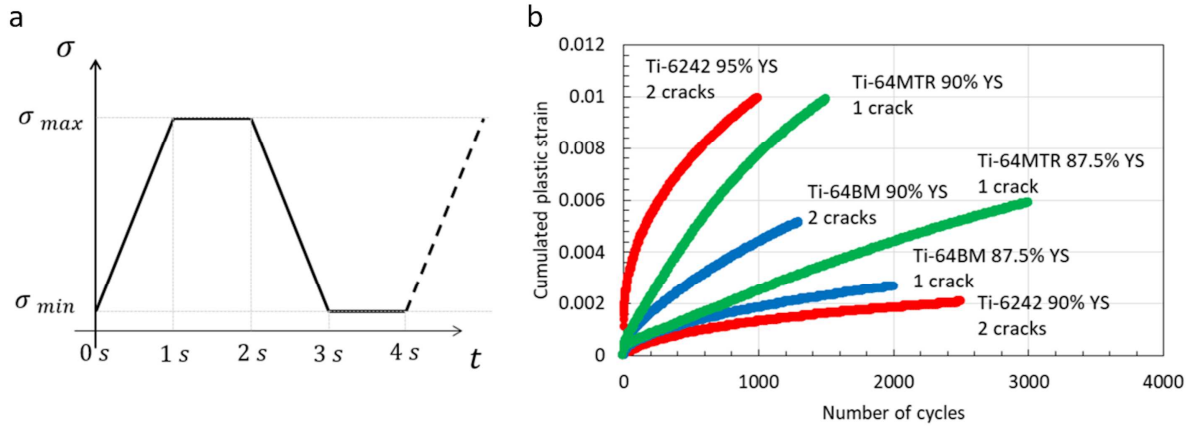

Figure 2: a. Schematic representation of the applied loading waveform during fatigue tests, and b. Cumulated plastic strain during the initial loading step plotted with respect to the number of cycles. The material, the number of cracks and the normalized peak stress as a fraction of the yield strength (YS) are indicated.

After the first test interruption, a TESCAN VEGA 3 SEM was used to detect microcracks. An automated routine was employed to map the whole gage length of the specimen (20 mm^2). Approximately 200 back-scattered electron micrographs with a 800 times magnification were taken for each specimen. The number of cracks identified for each test is indicated in figure 2b. A JEOL 7000F SEM was used to characterize the cracks and the surrounding microstructure at each test interruption. High magnification secondary electron and back-scattered electron micrographs are used to accurately locate the crack tip. The projected crack length, which corresponds to the length of the crack normal to the loading axis and reflects the driving force for growth, is derived at each step. The EBSD technique was used after the first test interruption to characterize local crystallographic orientations. A JEOL 6100 SEM equipped with a Hikari detector manufactured by EDAX was employed for that purpose. EBSD data collection was carried out using a step lower than 0.5 μm for all materials to obtain an accurate description of the microstructure. EBSD data was finally processed using the OIM Analysis software. One iteration of grain dilation with a threshold confidence index of 0.1 was applied to EBSD data to display orientation maps throughout the article. As crystallographic orientations can vary along a single crack growth increment, the average grain orientation, which was determined using a 2° threshold for grain boundary identification, was employed.

3. Results

3.1 Ti-64BM

Two Ti-64BM specimens were tested in the present study. 1300 cycles were initially applied on the Ti-64BM-1 specimen with a peak stress equivalent to 90 % of the yield strength and 2000 cycles were applied to the Ti-64BM-2 specimen with a peak stress equivalent to 87.5 %. After this first loading step, the Ti-64BM-1 specimen contained 2 cracks and the Ti-64BM-2 specimen contained 1 crack. The 3 cracks have nucleated at a (0001) twist boundary separating two primary α grains. Detailed characterization of the crack initiation sites and the associated nucleation mechanism are reported in [14]. Initial cracks ranged between 8.8 and 11.0 μm long. The initial crack length is thus similar to the average primary α grain size, which is about 12.4 μm. Sets of 300 cycles were then applied to the specimens until 2100 additional cycles to monitor crack growth. Micrographs showing the grown cracks at the end of the test are presented in figure 3. White

arrows indicate the locations of the crack tips at the end of the first step. Inverse pole figure maps showing the crystallographic orientation along the loading direction are also presented. The 2100 additional cycles have resulted in 3.5 µm and 11.3 µm growths in Ti-64BM-1 and 11.4 µm growth in Ti-64BM-2. It is worth noting that the longest crack is associated to crack growth across a cluster of primary α grains. Other cracks seemingly grew across transformed β regions. The crack length is plotted with respect to the additional number of cycles in figure 4a. The crack growths are quite well described using a linear relationship as highlighted by the high R^2 values. The increasing crack lengths do not seem to have a noticeable acceleration effect on the crack rate in the investigated regime. One can then assume that the variations such as shown in figure 4b result from the specificities of local microstructure arrangements.

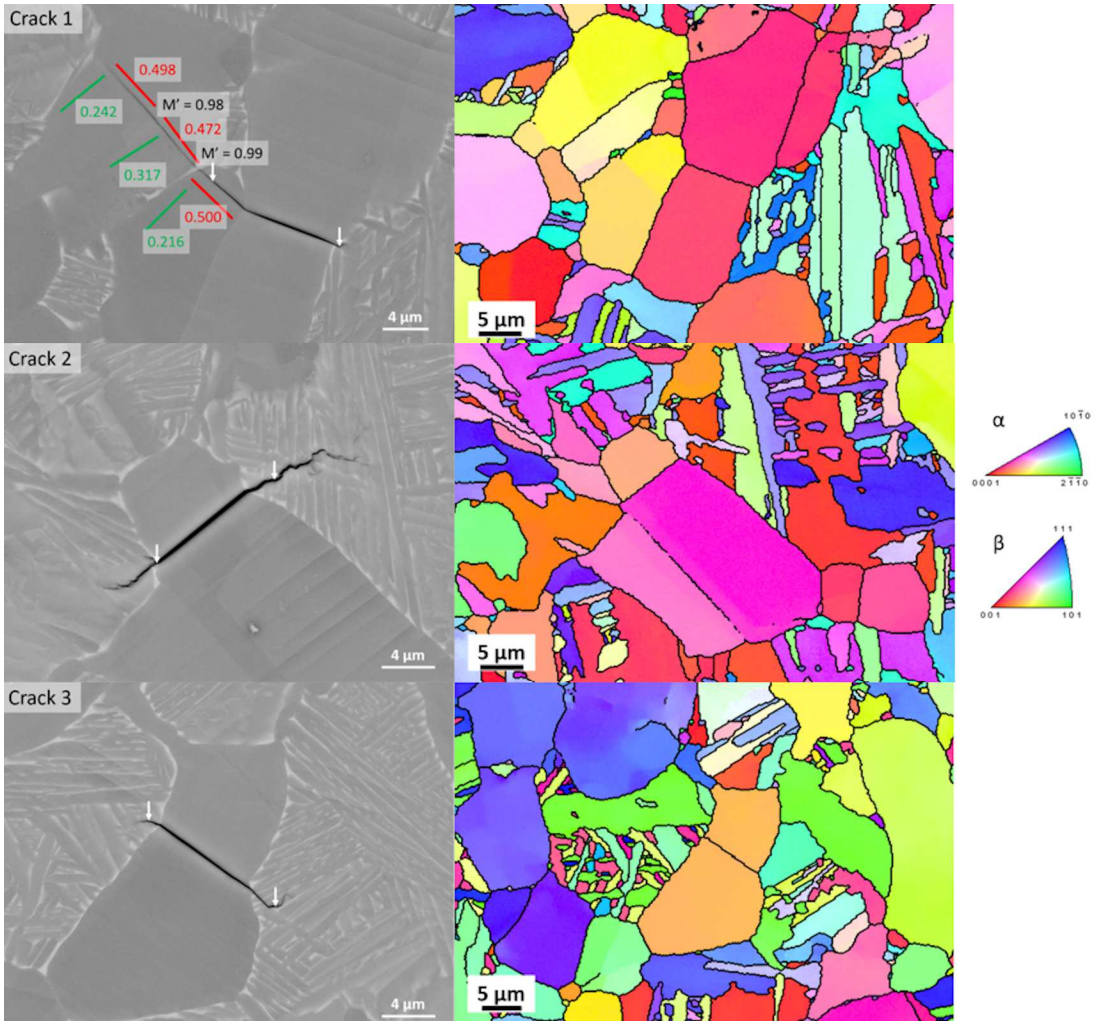

Figure 3: SEM micrographs of cracks in Ti-64BM at the final stage of growth. Basal and prismatic plane traces with the associated highest Schmid factor are indicated in primary α grains with red and green lines respectively. Misalignment between the crack planes are assessed using the *M'* parameter. Crack tip locations at the end of the first step are shown with white arrows. Inverse pole figure maps showing the crystallographic orientations along the loading direction (vertical) are presented.

Both sides of an initiated crack were occasionally observed to grow at significantly different rates. This is striking regarding Crack 1 shown in figure 3. The extensions at both crack tips are plotted in figure 4c as a function of the number of cycles. The crack extension could be up to five times longer on one side. These differences in evolution are likely to depend on microstructure. The crack growth rate is plotted with respect to the crack length in figure 4d. The color indicates whether primary α or transformed β regions are crossed. "Unkown" encompass mixed transformed β / primary α segments as well as unclear paths including boundaries and interfaces. The maximum crack growth rate was reached in a primary α grain on the left hand side of Crack 1 where the crack grew along a basal plane. The planes traces with the maximum Schmid

factor and the associated values for basal and prismatic slip systems are indicated in the cracked primary α grains. Basal and prismatic slip systems are considered as they are the main deformation systems operating in such Ti alloys [37,38]. The Schmid factor values indicate a high resolved shear stress acting on basal slip systems. The alignment between the crack planes across an interface or a boundary was also considered to analyze a potential correlation with the crack growth rates. The alignment between the basal planes in primary α grains was assessed using the *M'* parameter, defined as the cosine of the angle between basal planes normals. Values very close to 1 reveal a very good alignment from one grain to another. Although the lowest crack rates on this segment are associated with boundary crossing, limited variations indicate a minimal crack retardation at these boundaries. On the right hand side of Crack 1 shown in figure 3, the crack rate across transformed β was roughly five times slower. The comparison with other crack segments of Crack 2 and Crack 3 reveals that cracks grew faster in primary α grains with an average rate of 4.9 nm cycle^{-1} versus 0.7 nm cycle^{-1} in transformed β regions. Interestingly, the right hand side of Crack 2 extended through transformed β at a rate similar to the growth of Crack 1 across primary α. Sectioning parallel to the Ti-64BM specimen surface was carried out to unveil the subjacent microstructure surrounding Crack 2 and Crack 3. After a removal of 4 µm in depth, the micrographs shown in figure 5 were obtained. Primary α was present underneath the specimen surface on the side exhibiting the unexpectedly high crack growth rate and crack growth occurred along a well-aligned basal plane with a high Schmid factor. This observation reveals that these microstructural features provide a crack growth shortcut leading to a high apparent crack growth rates in transformed β regions. In contrast, surface and subsurface microstructural observations show that all other crack segments grew through transformed β. Taking this analysis into consideration, the crack extensions shown in figure 4c can be sorted out into two groups with drastically different propagation rates: "transformed β growth" or "primary α driven growth".

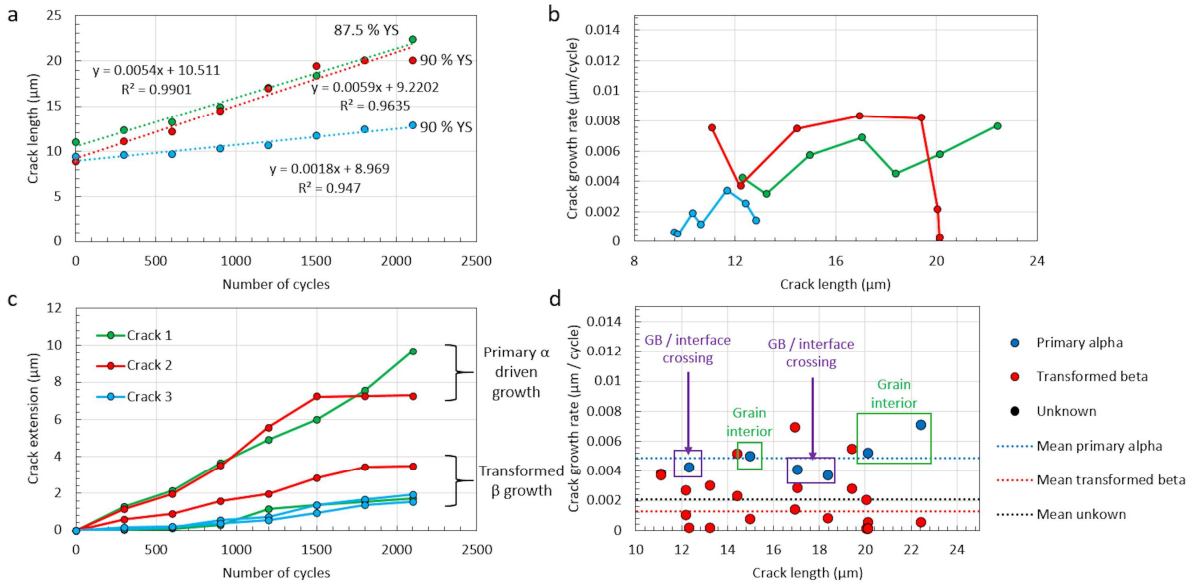

Figure 4: a. Crack length as a function of the number of cycles carried out beyond the initiation stage in Ti-64BM, b. Crack growth rate as a function of the total crack length, b. Crack extension on each side of the crack initiation site as a function of the number of cycles. Significantly different crack growth behaviors are visible. d. Crack growth rate on each side of the crack as a function of the crack length and the type of microstructural element crossed.

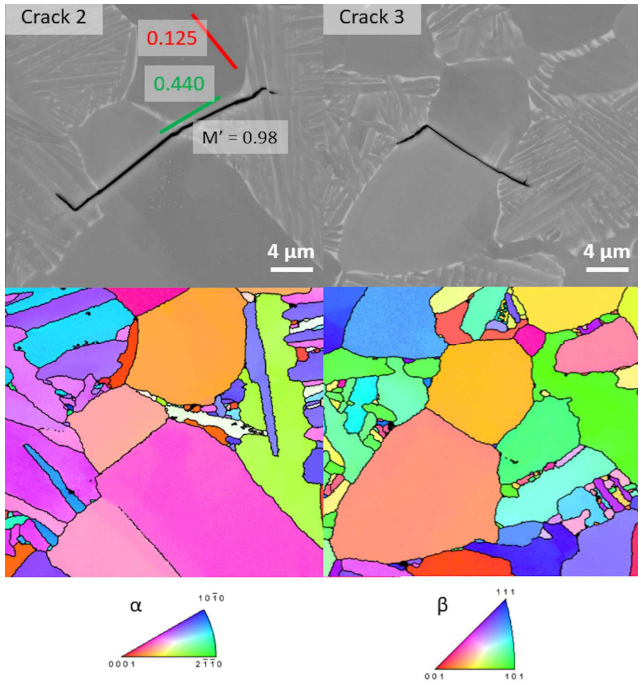

Figure 5: SEM micrographs and inverse pole figure maps showing the microstructure and the crystallographic orientation along the loading direction (vertical) 4 µm underneath the Ti-64BM-1 specimen surface shown in figure 3 for Crack 2 and Crack 3.

3.2 Ti-64MTR

Two specimens were tested with a peak stress equivalent to 90 % and 87.5 % of the yield strength. 1500 and 3000 cycles were initially applied. One crack was observed on the surface of each specimen. After the initial loading step, the cracks are 4.7 µm and 9.0 µm long. 2100 additional loading cycles were applied to each specimen and crack growth monitoring was carried out during interruptions in between sets of 300 cycles. SEM micrographs showing the cracks after the end of the tests are presented in figure 6. The crack length evolution is plotted with respect to the number of cycles in figure 7a. As observed in Ti-64BM specimens, the crack length display a linear evolution with the number of cycles. The slopes are in the 2.5 – 3 nm cycle^{-1} range. Significant variations in the crack rates are noticeable on the plot shown in figure 7b. The variations in crack growth rates are notably related to different crack growth processes occurring at the crack tips. Asymmetric growth is visible in figure 7c, where the extension on each side of the initial crack is plotted against the number of cycles. One side of each crack grew at a significantly higher rate than the other. The crack growth rate at each step is shown in figure 7d to discuss the role of microstructure on the crack growth behavior.

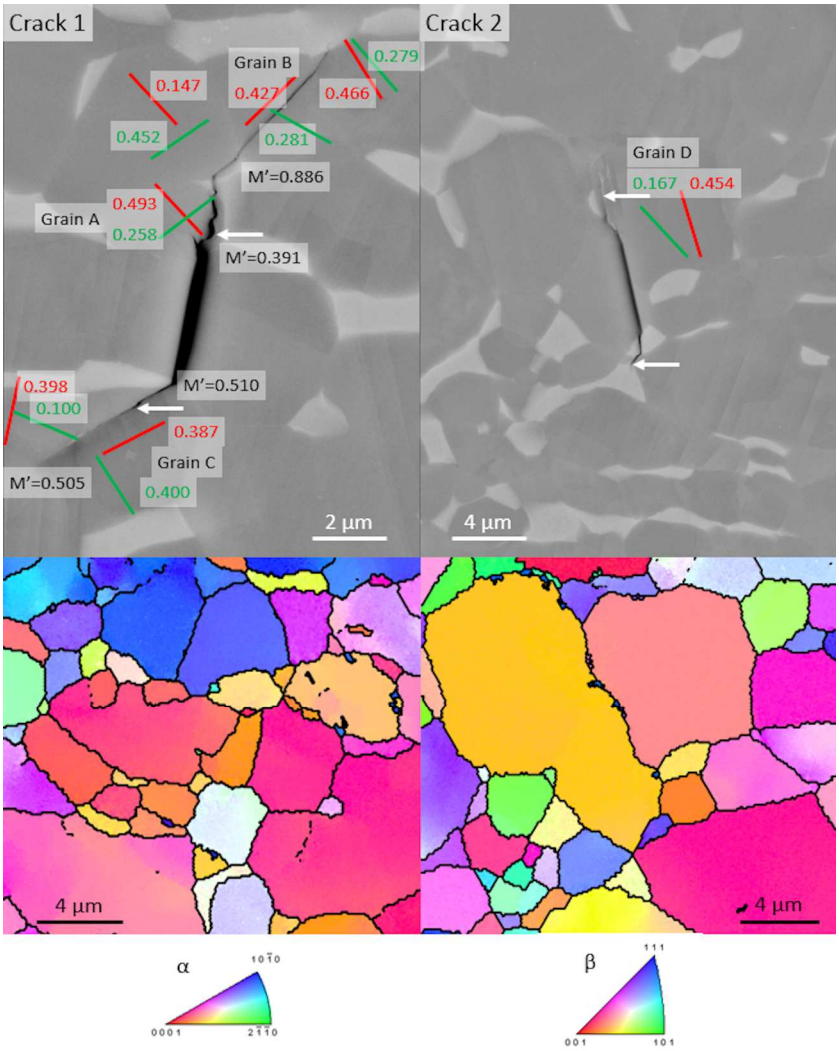

Figure 6: SEM micrographs of cracks at the final stage of growth in Ti-64MTR. Basal and prismatic plane traces with the associated highest Schmid factors are indicated in primary α grains with red and green lines respectively. Misalignment between the crack planes are assessed using the *M'* parameter. Crack tip locations at the end of the first step are shown with white arrows. Inverse pole figure maps showing the crystallographic orientations along the loading direction (horizontal) are also presented.

Regarding Crack 1 first, the upper crack segment has grown more quickly than the lower one. In the former, the crack has first crossed an α grain (denoted as Grain A) well orientated for basal slip as shown by the maximum Schmid factor for basal slip (i.e. 0.493). In this grain, the crack did not grow along the basal plane and the average crack rate is approximately 1.8 nm cycle^{-1}. In contrast, in Grain B where the maximum Schmid factor for basal slip is high too (i.e. 0.427), the crack grew at a rate around 6.2 nm cycle^{-1} along the basal plane. This difference in behavior can be rationalized considering the alignment between the crack planes on both sides of a boundary / interface. *M'* values are markedly different when the crack is entering Grain A (i.e. ≈ 0.391) or Grain B (i.e. ≈ 0.886). On the other side of the initiation site, in Grain C, the *M'* value was quite low as well and both basal and prismatic slip systems had similar and pretty high Schmid factors of 0.387 and 0.400 respectively. The crack grew along the basal plane at a rate below 1 nm cycle^{-1}. The difference with the crack growth behavior in Grain B highlights the critical role of the misalignment between the crack planes across the boundaries on the growth rate. Finally the crack stopped at a grain boundary with a poor alignment between basal planes, a high Schmid factor for basal slip but a very low value for prismatic slip. The other crack (Crack 2) exhibited crack branching on the upper segment, which mostly extends along basal planes with a high Schmid factor and a high *M'* value (≈ 1) in Grain D. The associated crack growth rate reaches 3.5 nm cycle^{-1}. Crack grew across β in the lower segment. The growth rate was around 0.3 nm cycle^{-1}, suggesting that β is associated with a low crack growth rate. However,

this observation must be taken with care as only one occurrence was considered and the associated growth rate leads to a pretty high measurement uncertainty.

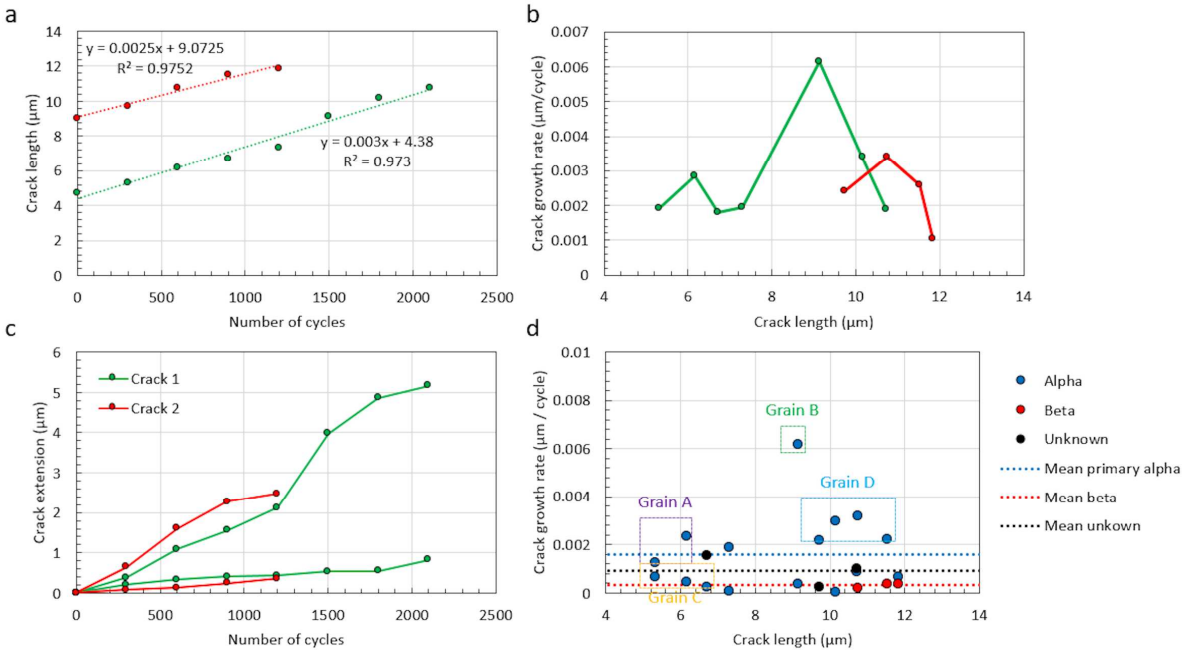

Figure 7: a. Crack length as a function of the number of cycles carried out beyond the initiation stage in Ti-64MTR, b. Crack growth rate as a function of the total crack length, c. Crack extension on each side of the crack initiation site as a function of the number of cycles. Significantly different crack growth behaviors are visible, and d. Crack growth rate on each side of the crack as a function of the crack length and the type of microstructural element crossed.

3.3 Ti-6242

A Ti-6242 specimen tested with a peak stress equivalent to 90 % of the yield strength was initially applied 2500 loading cycles. This specimen is denoted as Ti-6242-1 in the following. Resulting cracks are 13.9 µm and 15.4 µm long. 2000 additional cycles resulted in 6.8 and 13.5 µm crack growths respectively. The cracks at the final step are shown in figure 8. The crack length is plotted with respect to the number of cycles in figure 9a. The average growth rates are 3.6 nm.cycle^{-1} and 5.8 nm.cycle^{-1}. The slope in the plots indicates variable crack growth rates that depend on local microstructure. The crack growth rate is plotted against the crack length in figure 9b. The crack extensions at the tips of both cracks are plotted in figure 9c as a function of the number of cycles. At a given point, the crack extension could be up to four times longer on one side. As pointed out in previous paragraphs, both sides of an initiated crack were observed to occasionally grow at significantly different rates. This is striking regarding Crack 1 in figure 8 for instance. The crack extension rate at each tip of the cracks is shown in figure 9d. The color indicates the type of microstructural element crossed. "Unkown" encompass mixed transformed β / primary α segments as well as unclear paths including boundaries and interfaces. It is very obvious that cracks grew faster in primary α grains with an average rate of 2.9 nm cycle^{-1} versus 1.5 nm cycle^{-1} in transformed β regions. The difficult crack growth in transformed β regions is apparent on Crack 2 shown in figure 8.

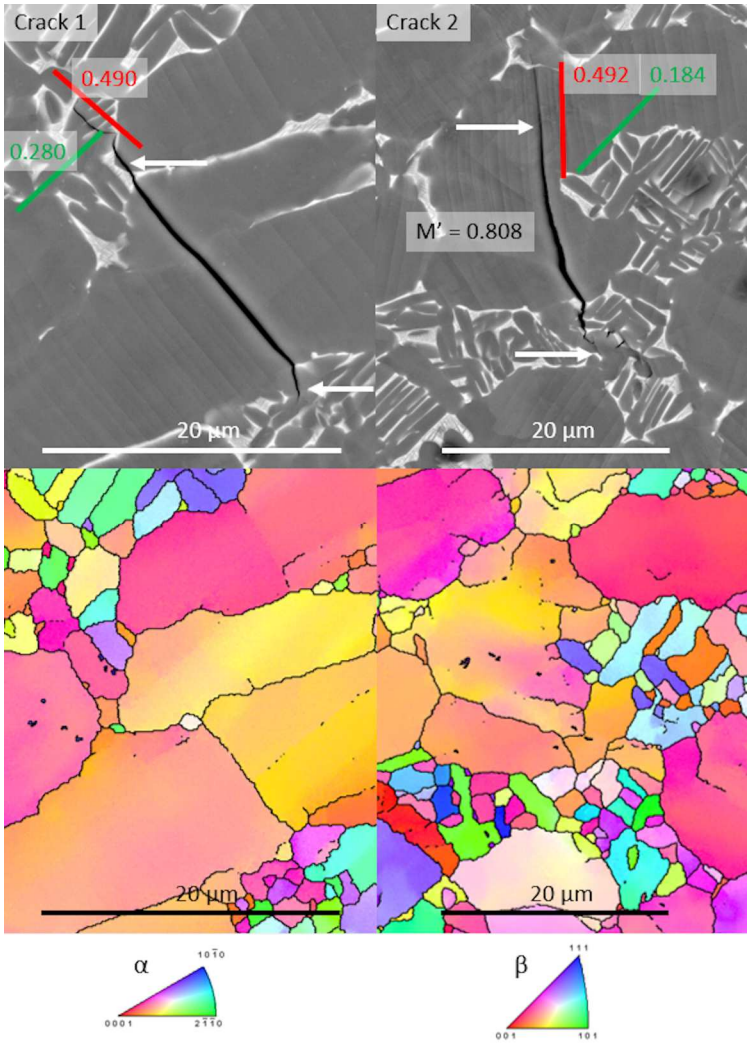

Figure 8: SEM micrographs of cracks at the final stage of growth in Ti-6242-1. Basal and prismatic plane traces with the associated highest Schmid factor are indicated in primary α grains with red and green lines respectively. Misalignment between the crack planes are given by the M' parameter. Crack tip locations at the end of the first step are shown with white arrows. Inverse pole figure maps showing the crystallographic orientations along the loading direction (horizontal) are also presented.

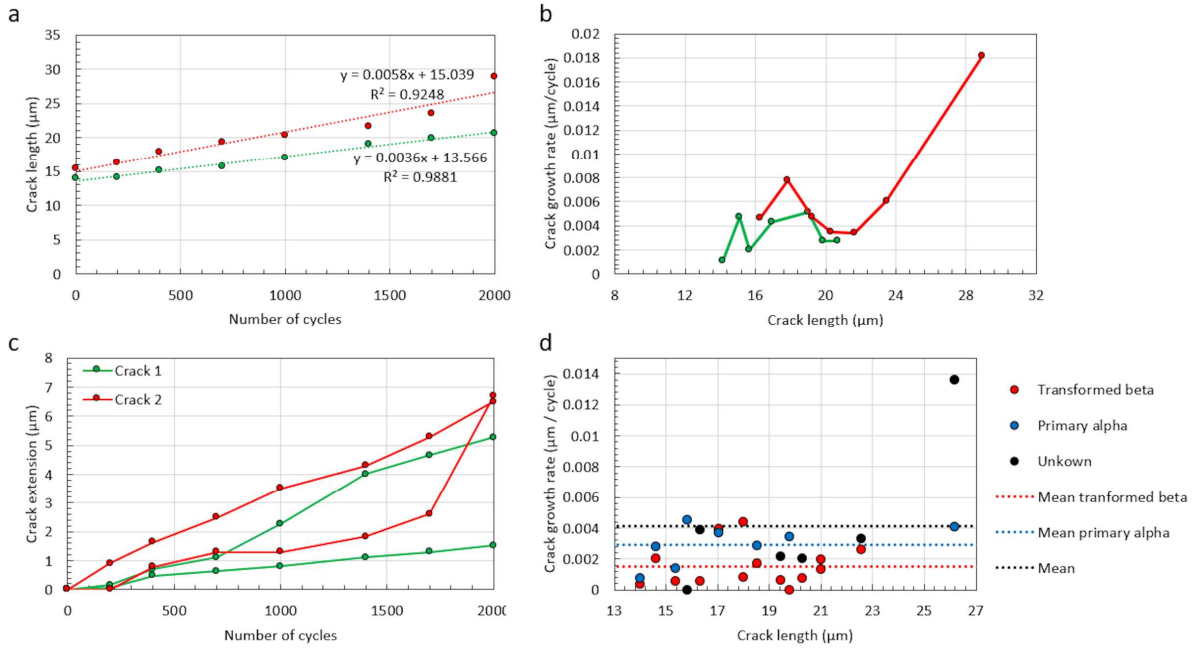

Figure 9: a. Crack length as a function of the number of cycles carried out beyond the initiation stage in Ti-6242-1, b. Crack growth rate as a function of the total crack length, c. Crack extension on each side of the crack initiation site as a function of the number of cycles. Significantly different crack growth behaviors are visible, and d. Crack growth rate on each side of the crack as a function of the crack length and the type of microstructural element crossed.

A few specific features from the plot in figure 9d are worth being highlighted. The maximum crack growth rate is about 14 nm cycle^{-1}. At this step, the newly formed crack segment seems disconnected from the main crack. While damage could have occurred away from the crack tip, one has to keep in mind that only 2D observations are carried out. Therefore, fast crack growth through the microstructure underneath the surface is likely to have occurred. However, this observation demonstrates that crack growth across the transformed β region, where the disconnection is observed, is difficult. The second highest crack growth rate segment involves cracking across primary α along a basal plane at a rate of 4.5 nm cycle^{-1}. A good alignment with the crack initiation segment is indicated by the calculated *M'* value (i.e. 0.808). Regarding transformed β regions, the highest crack rate is noticed in a colony. The value is approximately 4.4 nm cycle^{-1}. The crack grew along a basal plane without deflection across the multiple lamellas with similar orientations. This shows that minimal crack retardation can occur in lamellar region. Unfortunately the M' value could not be determined because of a high uncertainty in the incoming crack plane.

3.4 Ti-6242 and dwell sensitivity

A similar experiment was carried out to investigate the effect of load holds on the small crack growth behavior. The Ti-6242-2 specimen was initially tested with 1000 fatigue cycles using a peak stress equivalent to 95 % of the yield strength. Sets of 100 dwell-fatigue cycles were inserted in between sets of 200 fatigue cycles. With the exception of the load hold period at peak stress, which is set at 120 s for dwell-fatigue cycles and 1 s for fatigue cycles, all other parameters of the loading waveform were similar. Such numbers of cycles ensure low crack growth increments, thus allowing the analysis of fatigue and dwell-fatigue crack growth across similar microstructural configurations. The cracks at the final step are shown in figure 10. The crack length is plotted with respect to the number of cycles in figure 11a. The initial crack lengths are 4.8 µm and 6.9 µm. After 1800 additional cycles, the cracks are 15.3 µm and 20.5 µm long respectively. The average crack growth rates are 6.1 and 7.9 nm.cycle^{-1}. The average crack growth rate is about 11.2 nm.cycle^{-1} during dwell-fatigue loading versus 5.4 nm.cycle^{-1} during fatigue loading. The latter number is very close to the one found in the specimen subjected to fatigue loading only. This shows a

limited influence of the load holds on crack growth during fatigue loading segments as well as crack growth acceleration by a factor around 2 due to the introduction of load holds at peak stress.

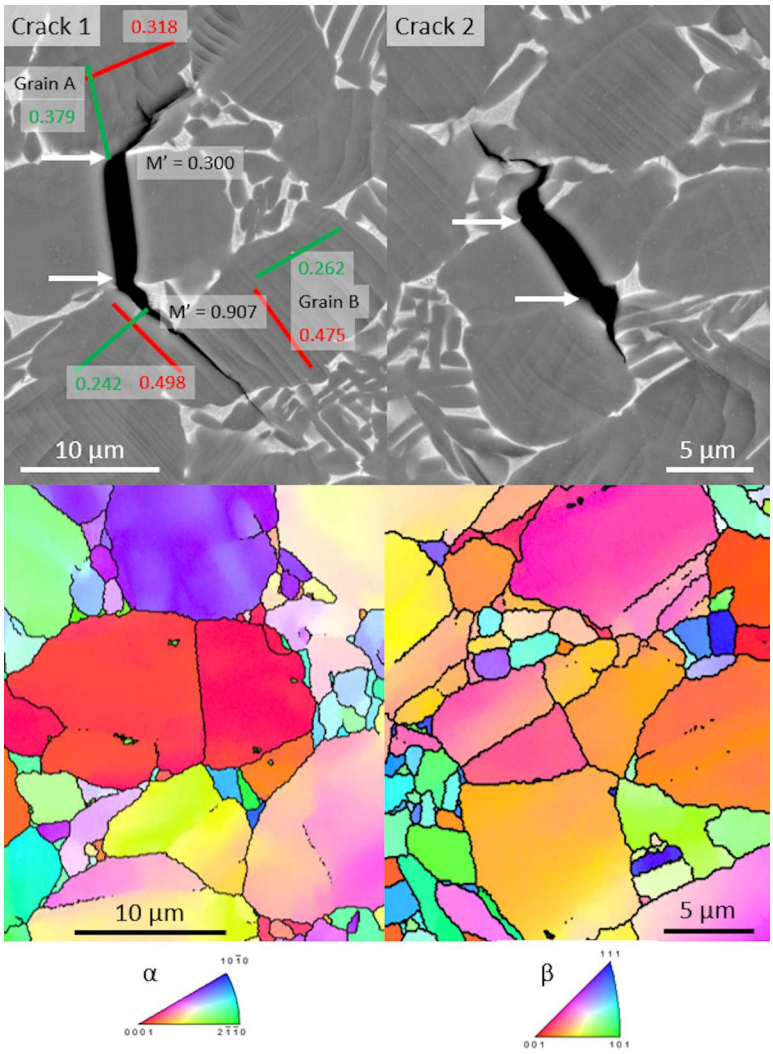

Figure 10: SEM micrographs of cracks at the final stage of growth in Ti-6242-2. Basal and prismatic plane traces with the associated highest Schmid factor are indicated in primary α grains with red and green lines respectively. Misalignment between the crack planes is assessed using the *M'* parameter. Crack tip locations at the end of the first step are shown with white arrows. Inverse pole figure maps showing the crystallographic orientations along the loading direction (horizontal) are also presented.

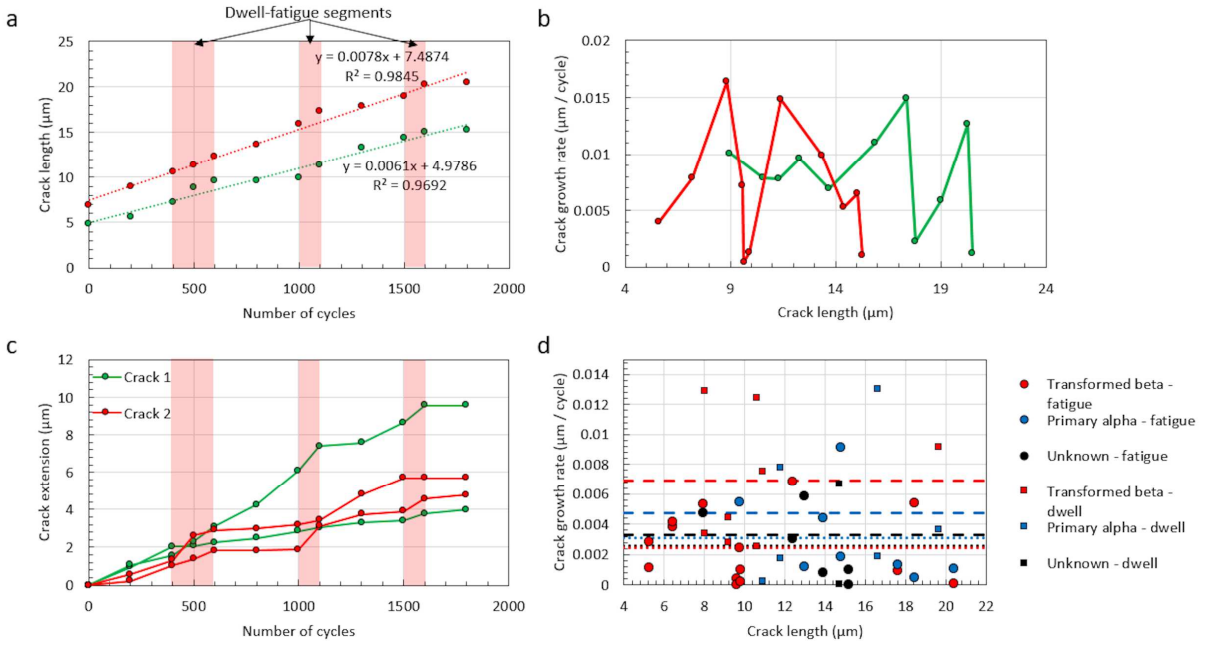

Figure 11: a. Crack length as a function of the number of cycles carried out beyond the initiation stage in Ti-6242-2, b. Crack growth rate as a function of the total crack length, c. Crack extension on each side of the crack initiation site as a function of the number of cycles. Significantly different crack growth behaviors are visible, and d. Crack growth rate on each side of the crack as a function of the crack length and the type of microstructural element crossed.

A high variability in crack growth rates is shown in figure 11b. In addition, higher values than for any other material tested with fatigue loadings are reached. These differences are associated with a significant crack growth asymmetry which can be observed using the crack extension plot presented in figure 11c. Local crack growth rate values are shown in figure 11d depending on the loading and the microstructural element crossed. The maximum growth rate is observed in primary α during a dwell-fatigue segment and crack growth rates higher than 10 nm.cycle^{-1} are only reached during dwell-fatigue segments. This observation highlights the faster crack growth rate due to the load hold at peak stress. This is observed for all kinds of microstructural elements. The average crack growth rate in primary α is 4.7 nm.cycle^{-1} during dwell-fatigue loading versus 3.1 nm.cycle^{-1} during fatigue loading. In transformed β, the average growth rate is about 6.9 nm.cycle^{-1} during dwell-fatigue loadings versus 2.4 nm.cycle^{-1} during fatigue loadings. It can be surprising to notice that crack acceleration could be higher in transformed β regions as lamellar microstructures are deemed more resistant to cold dwell [39]. In agreement with this observation, a higher crack growth rate was also reported in microstructural regions containing a high transformed β fraction [40]. However, one has to keep in mind that a limited number of steps and cracks were considered in the present study.

4. Discussion

4.1 Methods employed, advantages and limitations

The growth of naturally formed small fatigue cracks was monitored ex situ using interrupted cyclic loadings and SEM characterization. With this approach, significant variations in crack growth rates depending on microstructural features and loading conditions were observed. In particular, direct crack growth monitoring with alternating fatigue and dwell-fatigue segments allowed to assess crack rates within similar microstructural environments for both loading waveforms, which is generally difficult when studied using different specimens. Although several salient findings have been obtained and worth being highlighted, the results presently obtained are insufficient to obtain an exhaustive overview of the relations between crack growth and microstructure. Indeed, a restricted amount of microstructural configurations have been considered notably because of i. the time consuming nature of such experiments, and ii. the

intrinsic propensity of a restricted set of microstructural configurations to be potential crack initiation sites [41]. In addition, surface observations imply strong hypotheses about the 3D geometry of the crack and the effect of subsurface microstructure. This is especially important as the present work highlighted the importance of the 3D microstructure on the small crack growth behavior. The existence of fast growth paths in 3D, which have a key contribution to the overall crack growth behavior, suggests that a correct prediction can only be reached using 3D models and simulations. However, the spatial resolution of SEM allows an accurate and direct estimation of the crack tip location, which is key to investigate microstructural effects in materials with a small microstructure characteristic length scale such as Ti alloys and still far from nowadays standards in resolution considering X-ray tomography techniques for instance.

4.2 Crack initiation, small crack growth, fatigue life and dwell-fatigue life debits

As shown in this study, crack nucleation in the Ti-64BM material proceeds in less than 1300 cycles with a peak stress equivalent to 90 % of the yield strength. The fatigue life to crack nucleation was estimated using an assessment of the number of cycles required for the crack to extend from the initiation (0001) twist boundary to the state observed after 1300 cycles. The average growth rate shown in figure 4a was used for this purpose. The life to crack nucleation is about 707 cycles for Crack 1 and 828 cycles for Crack 2. The total lifetime is about 1.1 x 10^4 cycles according to prior work involving the same material and loading [11]. The crack nucleation stage thus accounts for approximately 7 - 8 % of the fatigue life with these conditions. As the fastest growing crack has extended over roughly 15 μm in 2000 applied cycles, the microstructurally small crack growth regime has a major contribution to the fatigue lifetime with the presently applied testing conditions. It is worth noting that such applied peak stress levels can lead to dwell-fatigue life debits by a factor of 3 when the load hold is increased from 1 s to 120 s [11]. This highlights the importance to consider both crack nucleation and growth stages to assess fatigue lives and associated dwell-fatigue life debits.

Dwell-fatigue failure is generally associated to specific features such as substantial strain accumulation, subsurface crack initiation, facetted fracture surfaces matching microtextured regions and dwell-fatigue life debits that can exceed a factor of 10. However, materials such as Ti-6Al-2Sn-4Zr-6Mo or Ti407 that display a low sensitivity to dwell time, do not exhibit these features under dwell-fatigue loading [36,42]. Features of fatigue failure such as surface crack initiation are typically exhibited alongside limited but substantial life debits (i.e. up to a factor 2 to 3) [36]. The crack nucleation life being roughly 10 % of the total fatigue lifetime, the worst-case scenario involving surface crack nucleation at the first cycle promoted by cold creep followed by fatigue like crack growth would result in a 10 % lifetime reduction. A reduction in crack nucleation life alone is thus unable to account for dwell-debits by a factor of 2 or 3. Accelerated crack growth, which is the main contributor to the fatigue lifetime, is thus likely to play a major role. Contrasting results about the role of dwell time on long crack growth have been reported in the literature [43,44]. However, crack closure corrected data suggests a noticeable increase in growth rates with the introduction of dwell periods at peak stress [45]. Comparison of cracks growing in air revealed higher growth rates by a factor about 2. To the best of the authors' knowledge, the regime of naturally initiated small crack growth is less documented. The present work demonstrates that acceleration by a factor about 2 occurs with load hold periods increased from 1 s to 120 s. This is consistent with lifetime reductions encountered using cyclic loadings including load holds and associated with fatigue like fracture features.

Higher dwell-fatigue life debits, by a factor of 10 or higher, can also occur in dwell sensitive materials subjected to appropriate loading conditions. A switch from surface to internal crack nucleation is generally observed to occur. Hard grains, which are poorly oriented for plastic deformation, are held responsible for a fast and unimpeded dwell-fatigue crack growth and account for a major part of the lifetime reductions, especially if gathered in microtextured regions [16,46]. However, prior studies have shown that dwell-fatigue life debits can occur even in the absence of hard grains [47]. With the present results, we provide an explanation to the observed debits in microstructures lacking hard grains: lifetimes are reduced due to small crack acceleration during load holds, even in α grains where <a> slip operates. However, the observed accelerations are quite small as compared to previously reported for [0001] oriented MTRs. In addition, one may argue that these tests are carried out in air and considering surface cracks that may not accurately represent subsurface dwell-fatigue cracks. A similar acceleration might be expected under high vacuum as

observed for longer cracks [45], nevertheless the stress state at the crack tip may differ and modulate the extent of the dwell effect. Although further investigations are needed regarding this aspect, the substantial small crack acceleration during load holds implies a reduced number of cycles required to reach the long crack behavior and is expected to have a key contribution to the dwell-fatigue life debits.

4.3 Microstructure and small crack growth

The crack growth rate was presently observed to be substantially higher in primary α than in transformed β for both investigated alloys. It is worth noting that the slip length in the former microstructural elements is generally higher. As a consequence, the density of grain boundaries / interface hindering crack growth is lower in α grains. The average crack growth rates in equiaxed α and transformed β regions for all investigated materials are plotted in figure 12 against the α grain / colony size which defines the slip length. Interestingly, equiaxed α in Ti-64MTR and transformed β in Ti-6242 and Ti-64BM exhibit similar slip lengths and average crack rates. This observation suggests that the slip length is more important than the type of microstructural element that is crossed (α grain / lamellar transformed β). This is also confirmed by the fast crack advance noticed in lamellar colonies of Ti-6242 shown in figure 8 (Crack 1) and 8d, at a rate similar to those encountered in primary α. Higher average crack growth rates were observed in primary α in Ti-64BM and Ti-6242, which suggests that the increased slip length favors a faster crack growth. However, one has to keep in mind that a limited set of microstructural configurations has been considered for each material and other parameters, such as preferential crystallographic orientations, may influence this trend, or at least the slope of the presently reported linear regression.

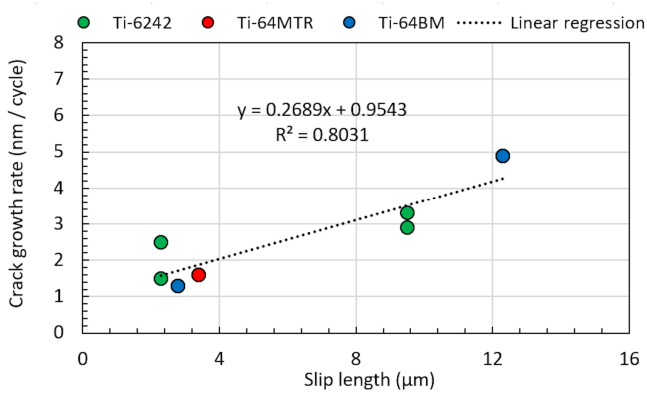

Figure 12: Average fatigue crack growth rate with respect to the slip length, which is taken equal to the α grain size or to the colony size depending on the alloys and microstructures.

A high maximum Schmid factor for basal slip, which indicates a high resolved shear stress on a basal slip system, was generally found associated with high crack growth rates for all investigated materials. The crack growth rates in primary α grains are plotted with respect to the maximum Schmid factor for basal slip in figure 13a. From this plot, it is obvious that high crack rates are reached provided a high resolved shear stress is acting on a basal slip system. Plotting data against the maximum Schmid factor for prismatic slip does not lead to a similar observation as shown in figure 13b. Some observations, such as Grain A in figure 10 or Grain C in figure 6, suggests that cross-slip and multiplicity of active slip modes may blunt the crack and reduce the growth rate. Additional data is needed to confirm this trend. However, the crystallographic texture in the crack initiation regions implied that α grains neighboring the crack nucleation site were generally well oriented for basal slip. This is evident in the plot of figure 13c where the crack rates are displayed as a function of the misalignment between the c-axis of the HCP lattice and the loading direction. Most values are located near 45°, which corresponds to the maximum Schmid factor value for basal slip.

The misalignement between the incoming crack and the basal plane was calculated, when the incoming crack plane was known. As a consequence, a subset of the data shown in figure 13a, 13b or 13c was considered. High crack growth rates were found to occur provided a good alignment exists between

the incoming crack and the basal plane, which generally experienced a high resolved shear stress. Crack rates are plotted as a function of the *M'* parameter in figure 13d. In spite of a limited amount of data, a strong correlation between the alignment and the crack growth rate is obtained. The data shows that *M'* around or above 0.8 favors fast growth. This value corresponds to a misalignment about 37° between plane normals, which is consistent with the critical slip plane misalignment for slip transfer to occur [48]. This key role of misalignment can be easily rationalized through 3D consideration of crack growth. If the incoming crack is not well aligned, basal plane cracking alone is not able to accommodate the 3D geometry of the incoming crack and cracking along other planes has to occur. This is likely to prevent fast crack growth.

To summarize, a high resolved shear stress acting on the basal plane and a good alignment between the incoming crack and the highly stressed potential crack plane are required for fast crack growth. These features suggest that the crack growth along basal planes is mainly driven by mode II growth and governed by the resolved shear stress rather than the normal stress, which would result in maximum crack growth rates for low angles between the c-axis of the HCP lattice and the loading direction. These results are in good agreement with the recent findings of Koyama et al. [24].

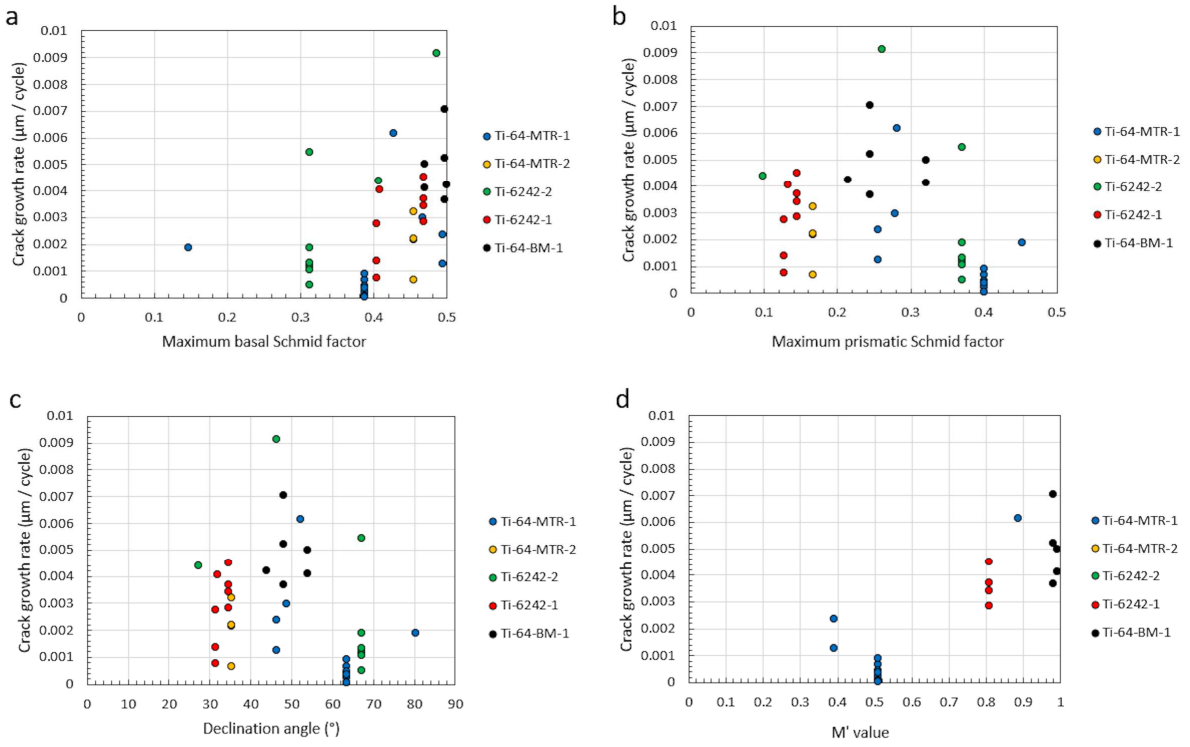

Figure 13: Crack growth rates in equiaxed α with respect to the maximum Schmid factor for a. basal slip and b. prismatic slip, c. Crack growth rates in equiaxed α with respect to the misorientation between the c-axis of the HCP lattice and the loading direction and d. Crack growth rates in equiaxed α with respect to the *M'* values, indicating the relation between the crack growth rate and the alignment with the incoming crack.

4.4 Implications on the fatigue of Ti alloys

The fastest growth was noticed in α grain clusters with the following features: high resolved shear stress acting on a basal slip system and a good alignment between the incoming crack and the basal plane. In addition, the cracks were observed to be only moderately slowed down when crossing interface / boundaries with low misorientations. Prior work involving post mortem analysis of failed specimen have highlighted such configurations to be associated with poor fatigue performance [8]. The present study thus brings direct experimental evidence of the detrimental influence of microtextured α grain clusters favorably oriented for basal slip on the small crack growth resistance. More generally, a high degree of microtexture is thus expected to induce reduced fatigue lives through offering fast crack growth opportunities at the

millimeter scale. This deleterious effect adds to the pronounced stress and strain heterogeneities arising from non-random spatial distribution of crystallographic orientations [49,50]. In contrast, transformed β regions were presently found efficient barriers for fast microcrack growth. This observation is consistent with previously reported trends [21]. However, as the weakest link governs the fatigue properties, the fatigue lifetime is likely to be sensitive to the existence of isolated α grain clusters, which can induce accelerated crack growth by a factor of 2 to 5 over a given length. Such heterogeneities in the microstructural configurations are likely to determine the outgrowing crack in case multiple cracks initiate or contribute to the high variability in fatigue lives reported in Ti alloys [7]. As a consequence, a specific attention must be paid to the existence of α grain clusters and further efforts applied toward optimized processing routes to avoid their occurrence in bi-modal microstructures. One way to do so is to reduce the fraction of primary α, which is known to lead to improved fatigue lives [21].

5. Conclusions

The early growth of small cracks was studied in different Ti alloys with various microstructures. Fatigue and dwell-fatigue loadings were repeatedly interrupted and crack growth was monitored using SEM. Natural cracks initiated at (0001) twist boundaries were considered in this work. The main findings are listed in the following:

- Microstructure heterogeneities surrounding the crack nucleation site induced a variability in small crack growth rate which can exceed a factor of 3 for a given material. This confirms the role of the small crack growth as a major root cause of scatter in fatigue life.
- The average growth rate is several times faster in primary α grains than in transformed β regions. The data suggests that higher slip length in α grains is a key feature. As a consequence, clusters of primary α play a key role to determine the dominant crack in bi-modal microstructures, if multiple cracks are initiated, or the lifetime and the associated scatter, if a single crack is initiated.
- The highest crack growth rates were observed along basal planes with a high resolved shear stress and well aligned with the incoming crack plane. This is consistent with mode II crack growth along the basal planes.
- Minimal crack retardations were observed across grain boundaries associated to well-aligned slip planes. This implies a detrimental influence of microtextured regions on the fatigue performance.
- Under dwell-fatigue loading condition, the small crack growth rates are accelerated by a factor of 2 in average as the hold time at peak stress is increased from 1 s to 120 s despite the lack of hard grains. Reductions in lifetimes due to load holds are expected to be tightly related to small crack growth acceleration such as observed in this study.

Acknowledgements

This work has been partially supported by « Nouvelle Aquitaine » Region and by European Structural and Investment Funds (ERDF reference : P-2016-BAFE-94/95). Pprime Institute gratefully acknowledges "Contrat de Plan Etat - Région Nouvelle-Aquitaine" (CPER) as well as the "Fonds Européen de Développement Régional (FEDER)" for their financial support to the reported work.

References

[1] J.C. Williams, R.R. Boyer, Opportunities and Issues in the Application of Titanium Alloys for Aerospace Components, Metals. 10 (2020) 705. https://doi.org/10.3390/met10060705.

[2] M.R. Bache, A review of dwell sensitive fatigue in titanium alloys: the role of microstructure, texture and operating conditions, International Journal of Fatigue. 25 (2003) 1079–1087. https://doi.org/10.1016/S0142-1123(03)00145-2.

[3] X. Demulsant, J. Mendez, MICROSTRUCTURAL EFFECTS ON SMALL FATIGUE CRACK INITIATION AND GROWTH IN Ti6A14V ALLOYS, Fatigue & Fracture of Engineering Materials & Structures. 18 (1995) 1483–1497. https://doi.org/10.1111/j.1460-2695.1995.tb00870.x.
[4] J.A. Hall, Fatigue crack initiation in alpha-beta titanium alloys, International Journal of Fatigue. 19 (1997) 23–37. https://doi.org/10.1016/S0142-1123(97)00047-9.
[5] R.K. Nalla, R.O. Ritchie, B.L. Boyce, J.P. Campbell, J.O. Peters, Influence of microstructure on high-cycle fatigue of Ti-6Al-4V: Bimodal vs. lamellar structures, Metall Mater Trans A. 33 (2002) 899–918. https://doi.org/10.1007/s11661-002-0160-z.
[6] H. Knobbe, P. Köster, H.-J. Christ, C.-P. Fritzen, M. Riedler, Initiation and propagation of short fatigue cracks in forged Ti6Al4V, Procedia Engineering. 2 (2010) 931–940. https://doi.org/10.1016/j.proeng.2010.03.101.
[7] S.K. Jha, C.J. Szczepanski, P.J. Golden, W.J. Porter, R. John, Characterization of fatigue crack-initiation facets in relation to lifetime variability in Ti–6Al–4V, International Journal of Fatigue. 42 (2012) 248–257. https://doi.org/10.1016/j.ijfatigue.2011.11.017.
[8] V. Sinha, A.L. Pilchak, S.K. Jha, W.J. Porter, R. John, J.M. Larsen, Correlating Scatter in Fatigue Life with Fracture Mechanisms in Forged Ti-6242Si Alloy, Metall Mater Trans A. 49 (2018) 1061–1078. https://doi.org/10.1007/s11661-017-4437-7.
[9] C.J. Szczepanski, S.K. Jha, J.M. Larsen, J.W. Jones, Microstructural Influences on Very-High-Cycle Fatigue-Crack Initiation in Ti-6246, Metall Mater Trans A. 39 (2008) 2841–2851. https://doi.org/10.1007/s11661-008-9633-z.
[10] S. Joseph, T.C. Lindley, D. Dye, Dislocation interactions and crack nucleation in a fatigued near-alpha titanium alloy, International Journal of Plasticity. 110 (2018) 38–56. https://doi.org/10.1016/j.ijplas.2018.06.009.
[11] C. Lavogiez, S. Hémery, P. Villechaise, On the mechanism of fatigue and dwell-fatigue crack initiation in Ti-6Al-4V, Scripta Materialia. 183 (2020) 117–121. https://doi.org/10.1016/j.scriptamat.2020.03.031.
[12] M.R. Bache, M. Cope, H.M. Davies, W.J. Evans, G. Harrison, Dwell sensitive fatigue in a near alpha titanium alloy at ambient temperature, International Journal of Fatigue. 19 (1997) 83–88. https://doi.org/10.1016/S0142-1123(97)00020-0.
[13] F. Bridier, P. Villechaise, J. Mendez, Analysis of the different slip systems activated by tension in a α/β titanium alloy in relation with local crystallographic orientation, Acta Materialia. 53 (2005) 555–567. https://doi.org/10.1016/j.actamat.2004.09.040.
[14] S. Hémery, J.C. Stinville, F. Wang, M.A. Charpagne, M. Emigh, T.M. Pollock, V. Valle, Strain Localization and Fatigue Crack Formation at (0001) Twist Boundaries in Titanium Alloys, Acta Materialia. (2021) 117227. https://doi.org/10.1016/j.actamat.2021.117227.
[15] A.L. Pilchak, Fatigue crack growth rates in alpha titanium: Faceted vs. striation growth, Scripta Materialia. 68 (2013) 277–280. https://doi.org/10.1016/j.scriptamat.2012.10.041.
[16] A.L. Pilchak, J.C. Williams, Observations of Facet Formation in Near-α Titanium and Comments on the Role of Hydrogen, Metall Mater Trans A. 42 (2011) 1000–1027. https://doi.org/10.1007/s11661-010-0507-9.
[17] S. Suresh, R.O. Ritchie, Propagation of short fatigue cracks, International Metals Reviews. 29 (1984) 445–475. https://doi.org/10.1179/imtr.1984.29.1.445.
[18] P. Chowdhury, H. Sehitoglu, Mechanisms of fatigue crack growth – a critical digest of theoretical developments, Fatigue & Fracture of Engineering Materials & Structures. 39 (2016) 652–674. https://doi.org/10.1111/ffe.12392.
[19] K.S. Chan, J. Lankford, The role of microstructural dissimilitude in fatigue and fracture of small cracks, Acta Metallurgica. 36 (1988) 193–206. https://doi.org/10.1016/0001-6160(88)90038-7.
[20] M.J. Caton, R. John, W.J. Porter, M.E. Burba, Stress ratio effects on small fatigue crack growth in Ti–6Al–4V, International Journal of Fatigue. 38 (2012) 36–45. https://doi.org/10.1016/j.ijfatigue.2011.11.004.
[21] G. Lütjering, Influence of processing on microstructure and mechanical properties of (α+β) titanium alloys, Materials Science and Engineering: A. 243 (1998) 32–45. https://doi.org/10.1016/S0921-5093(97)00778-8.
[22] M. Hassanipour, S. Watanabe, K. Hirayama, H. Toda, K. Uesugi, A. Takeuchi, Short crack growth behavior and its transitional interaction with 3D microstructure in Ti-6Al-4V, Materials Science and Engineering: A. 738 (2018) 229–237. https://doi.org/10.1016/j.msea.2018.09.073.

[23] M. Peters, A. Gysler, G. LÜtjering, Influence of texture on fatigue properties of Ti-6Al-4V, Metall Mater Trans A. 15 (1984) 1597–1605. https://doi.org/10.1007/BF02657799.
[24] A. Maenosono, M. Koyama, Y. Tanaka, S. Ri, Q. Wang, H. Noguchi, Crystallographic selection rule for the propagation mode of microstructurally small fatigue crack in a laminated Ti-6Al-4V alloy: Roles of basal and pyramidal slips, International Journal of Fatigue. 128 (2019) 105200. https://doi.org/10.1016/j.ijfatigue.2019.105200.
[25] C.M. Ward-Close, C.J. Beevers, The influence of grain orientation on the mode and rate of fatigue crack growth inα-titanium, Metall Mater Trans A. 11 (1980) 1007–1017. https://doi.org/10.1007/BF02654715.
[26] M.R. Bache, W.J. Evans, V. Randle, R.J. Wilson, Characterization of mechanical anisotropy in titanium alloys, Materials Science and Engineering: A. 257 (1998) 139–144. https://doi.org/10.1016/S0921-5093(98)00832-6.
[27] I. Bantounas, D. Dye, T.C. Lindley, The role of microtexture on the faceted fracture morphology in Ti–6Al–4V subjected to high-cycle fatigue, Acta Materialia. 58 (2010) 3908–3918. https://doi.org/10.1016/j.actamat.2010.03.036.
[28] I. Bantounas, D. Dye, T.C. Lindley, The effect of grain orientation on fracture morphology during high-cycle fatigue of Ti–6Al–4V, Acta Materialia. 57 (2009) 3584–3595. https://doi.org/10.1016/j.actamat.2009.04.018.
[29] M. Marx, W. Schäf, H. Vehoff, C. Holzapfel, Interaction of microcracks with selected interfaces: Focused ion beam for a systematic crack initiation, Materials Science and Engineering: A. 435–436 (2006) 595–601. https://doi.org/10.1016/j.msea.2006.07.042.
[30] K. Zhang, K.V. Yang, S. Lim, X. Wu, C.H.J. Davies, Effect of the presence of macrozones on short crack propagation in forged two-phase titanium alloys, International Journal of Fatigue. 104 (2017) 1–11. https://doi.org/10.1016/j.ijfatigue.2017.07.002.
[31] C.J. Szczepanski, S.K. Jha, J.M. Larsen, J.W. Jones, The Role of Local Microstructure on Small Fatigue Crack Propagation in an α + β Titanium Alloy, Ti-6Al-2Sn-4Zr-6Mo, Metall Mater Trans A. 43 (2012) 4097–4112. https://doi.org/10.1007/s11661-012-1228-z.
[32] W. Schäf, M. Marx, A.F. Knorr, Influence of microstructural barriers on small fatigue crack growth in mild steel, International Journal of Fatigue. 57 (2013) 86–92. https://doi.org/10.1016/j.ijfatigue.2012.11.006.
[33] Y.N. Lenets, R.S. Bellows, Crack propagation life prediction for Ti-6Al-4V based on striation spacing measurements, International Journal of Fatigue. 22 (2000) 521–529. https://doi.org/10.1016/S0142-1123(00)00019-0.
[34] A.L. Pilchak, A. Bhattacharjee, A.H. Rosenberger, J.C. Williams, Low ΔK faceted crack growth in titanium alloys, International Journal of Fatigue. 31 (2009) 989–994. https://doi.org/10.1016/j.ijfatigue.2008.03.036.
[35] M.E. Kassner, Y. Kosaka, J.S. Hall, Low-cycle dwell-time fatigue in Ti-6242, Metall and Mat Trans A. 30 (1999) 2383–2389. https://doi.org/10.1007/s11661-999-0246-y.
[36] J. Qiu, Y. Ma, J. Lei, Y. Liu, A. Huang, D. Rugg, R. Yang, A Comparative Study on Dwell Fatigue of Ti-6Al-2Sn-4Zr-xMo (x = 2 to 6) Alloys on a Microstructure-Normalized Basis, Metall Mater Trans A. 45 (2014) 6075–6087. https://doi.org/10.1007/s11661-014-2541-5.
[37] S. Hémery, P. Villechaise, On the influence of ageing on the onset of plastic slip in Ti-6Al-4V at room temperature: Insight on dwell fatigue behavior, Scripta Materialia. 130 (2017) 157–160. https://doi.org/10.1016/j.scriptamat.2016.11.042.
[38] C. Lavogiez, S. Hémery, P. Villechaise, Analysis of deformation mechanisms operating under fatigue and dwell-fatigue loadings in an α/β titanium alloy, International Journal of Fatigue. 131 (2020) 105341. https://doi.org/10.1016/j.ijfatigue.2019.105341.
[39] Titanium | Gerd Lütjering | Springer, (n.d.). https://www.springer.com/gp/book/9783540713975 (accessed September 10, 2020).
[40] A.L. Pilchak, A. Hutson, W.J. Porter, D. Buchanan, R. John, On the Cyclic Fatigue and Dwell Fatigue Crack Growth Response of Ti-6Al-4V, in: Proceedings of the 13th World Conference on Titanium, John Wiley & Sons, Ltd, 2016: pp. 993–998. https://doi.org/10.1002/9781119296126.ch169.
[41] C.P. Przybyla, D.L. McDowell, Simulated microstructure-sensitive extreme value probabilities for high cycle fatigue of duplex Ti–6Al–4V, International Journal of Plasticity. 27 (2011) 1871–1895. https://doi.org/10.1016/j.ijplas.2011.01.006.

[42] M. Bache, H. Davies, W. Davey, M. Thomas, I. Berment-Parr, Microstructural Control of Fatigue Behaviour in a Novel α + β Titanium Alloy, Metals. 9 (2019) 1200. https://doi.org/10.3390/met9111200.
[43] P.J. Bania, D. Eylon, Fatigue crack propagation of titanium alloys under dwell-time conditions, Metall Mater Trans A. 9 (1978) 847–855. https://doi.org/10.1007/BF02649795.
[44] C.A. Stubbington, S. Pearson, Effect of dwell on the growth of fatigue cracks in Ti-6Al-4V alloy bar, Engineering Fracture Mechanics. 10 (1978) 723–756. https://doi.org/10.1016/0013-7944(78)90030-9.
[45] P. Lefranc, C. Sarrazin-Baudoux, V. Doquet, J. Petit, Investigation of the dwell period's influence on the fatigue crack growth of a titanium alloy, Scripta Materialia. 60 (2009) 281–284. https://doi.org/10.1016/j.scriptamat.2008.09.033.
[46] A.L. Pilchak, A simple model to account for the role of microtexture on fatigue and dwell fatigue lifetimes of titanium alloys, Scripta Materialia. 74 (2014) 68–71. https://doi.org/10.1016/j.scriptamat.2013.10.024.
[47] M.C. Brandes, M.J. Mills, J.C. Williams, The Influence of Slip Character on the Creep and Fatigue Fracture of an α Ti-Al Alloy, Metall Mater Trans A. 41 (2010) 3463–3472. https://doi.org/10.1007/s11661-010-0407-z.
[48] S. Hémery, P. Nizou, P. Villechaise, In situ SEM investigation of slip transfer in Ti-6Al-4V: Effect of applied stress, Materials Science and Engineering: A. 709 (2018) 277–284. https://doi.org/10.1016/j.msea.2017.10.058.
[49] S. Hémery, A. Naït-Ali, M. Guéguen, J. Wendorf, A.T. Polonsky, M.P. Echlin, J.C. Stinville, T.M. Pollock, P. Villechaise, A 3D analysis of the onset of slip activity in relation to the degree of micro-texture in Ti–6Al–4V, Acta Materialia. 181 (2019) 36–48. https://doi.org/10.1016/j.actamat.2019.09.028.
[50] A. Nait-Ali, S. Hémery, M. Gueguen, How macrozone size and morphology influence yield in titanium alloys investigated using fast Fourier transform-based crystal plasticity simulations, International Journal of Solids and Structures. 216 (2021) 1–16. https://doi.org/10.1016/j.ijsolstr.2021.01.008.